

Spectral Enhancement and Pseudo-Anchor Guidance for Infrared-Visible Person Re-Identification

Yiyuan Ge^{1,†} Zhihao Chen^{1,†} Ziyang Wang^{2*} Jiaju Kang³ Mingya Zhang⁴

¹ Beijing Information Science And Technology University ² University of Oxford

³ Beijing Normal University ⁴ Nanjing University

1209027338@qq.com 2021011561@bistu.edu.cn ziyang.wang17@gmail.com

kjj_python@163.com dg20330034@smail.nju.edu.cn

Abstract—The development of deep learning has facilitated the application of person re-identification (ReID) technology in intelligent security. Visible-infrared person re-identification (VI-ReID) aims to match pedestrians across infrared and visible modality images enabling 24-hour surveillance. Current studies relying on unsupervised modality transformations as well as inefficient embedding constraints to bridge the spectral differences between infrared and visible images, however, limit their potential performance. To tackle the limitations of the above approaches, this paper introduces a simple yet effective Spectral Enhancement and Pseudo-anchor Guidance Network, named SEPG-Net. Specifically, we propose a more homogeneous spectral enhancement scheme based on frequency domain information and greyscale space, which avoids the information loss typically caused by inefficient modality transformations. Further, a Pseudo Anchor-guided Bidirectional Aggregation (PABA) loss is introduced to bridge local modality discrepancies while better preserving discriminative identity embeddings. Experimental results on two public benchmark datasets demonstrate the superior performance of SEPG-Net against other state-of-the-art methods. The code is available at <https://github.com/1024AILab/ReID-SEPG>.

Index Terms—Visible-infrared Person Re-identification, Spectral Enhancement, Pseudo-Anchor Guidance, Frequency Domain.

I. INTRODUCTION

Person Re-identification (ReID) has attracted significant attention due to its wide applications in security and surveillance, aiming to recognize individuals across different cameras and scenes [1, 2, 3, 4]. Traditionally, ReID tasks are primarily performed under visible light conditions. Visible-Infrared Person Re-identification (VI-ReID) extends this task to nighttime scenarios by leveraging multi-modality cameras, making it essential for real-world applications. Pedestrian images captured by infrared and visible cameras differ significantly as illustrated in Fig. 1(a). The infrared image highlights more distinct silhouette features, while the visible image provides richer color information. Fig. 1(b) illustrates the goal of VI-ReID is to match a query target from the hetero-modality gallery. The large spectral gap between infrared and visible images, however, poses severe challenges for this task.

Following the above concern, several pioneering studies [5, 6, 7, 8] maintain a pre-trained Generative Adversarial Network (GAN) to achieve mutual transformation between infrared and visible images. However, this unsupervised generation is

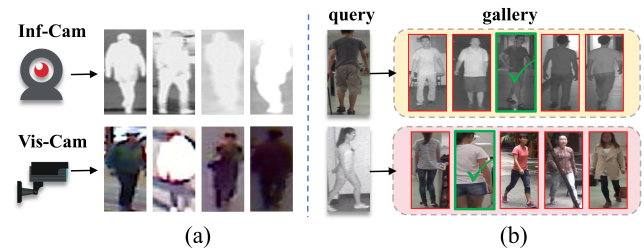


Fig. 1. (a) Visible and infrared images are captured by visible cameras and dedicated infrared cameras, respectively (example images from the RegDB dataset[20]). (b) A brief illustration of the VI-ReID task (example images taken from the SYSU-MM01 dataset[21]).

unstable, often compromising crucial modality information. Besides, other mainstream methods tackle the VI-ReID task by learning associative representations of infrared and visible images, using cross-centre losses to mitigate modality discrepancies [9, 10, 11, 12, 13]. Although these methods demonstrate effectiveness in some cases, certain limitations continue to hinder their performance. For example, [9, 10] only attempt to aggregate the centers of the two modalities, while [11] only focuses on intra-class center features and neglects modality categories. Moreover, these approaches tend to prioritize extracting modality-consistent representations while overlooking the distinctive identity embeddings.

To cope aforementioned issues, we propose a novel Spectral Enhancement and Pseudo-anchor Guidance Network (SEPG-Net) for the VI-ReID task. Unlike GAN-based approaches, we first transform RGB/visible features to a more homogeneous greyscale space. Following this, we extract the high-level semantic information from the frequency domain of the RGB images to enhance contour representations. Finally, Semantically Enhanced Grey (SEG) images are generated, which not only approximate the infrared modality but also maintain the original structural information of RGB images. The proposed method enhances cross-spectral features through a simple yet efficient design, which proves to be more conducive to network training against GAN-based methods. In addition, we improve the existing centre aggregation loss by introducing a unique Pseudo Anchor-guided Bidirectional Aggregation loss (PABA). The PABA loss learns cross-modality features at fine-

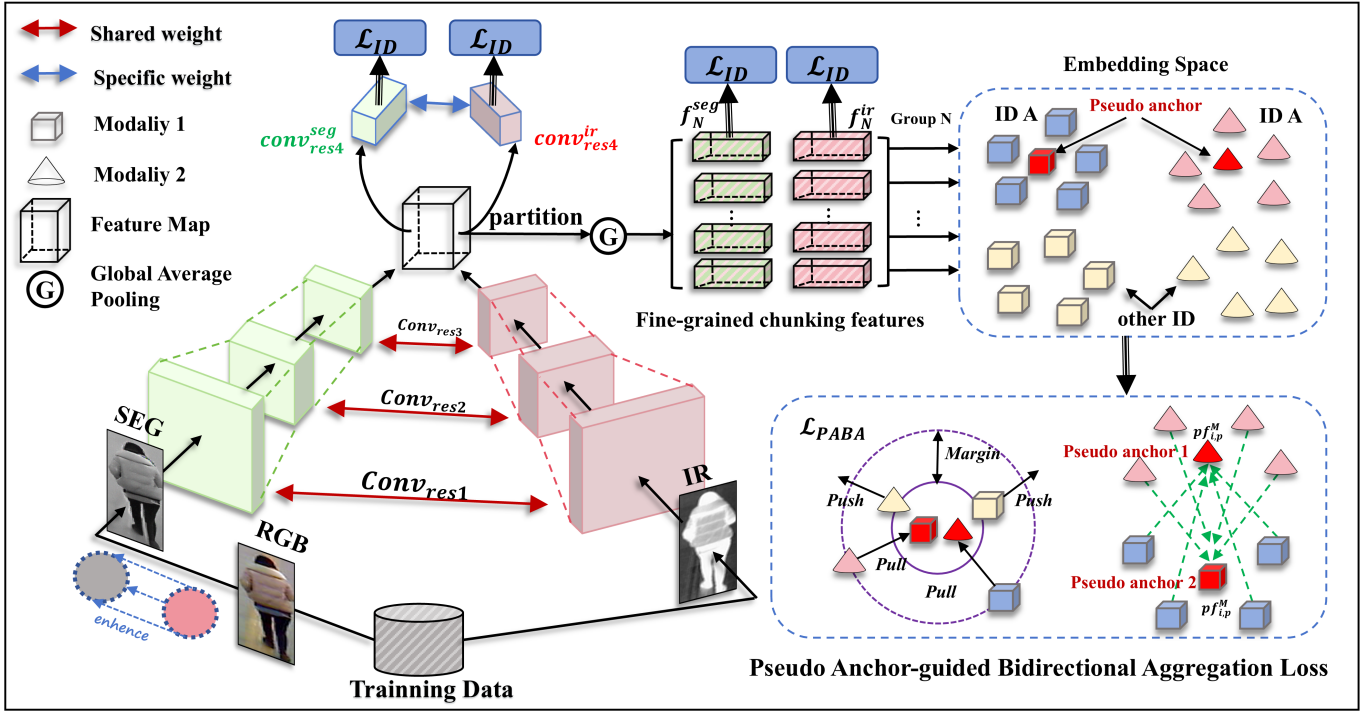


Fig. 2. The overall architecture of the proposed SEPG-Net. **First**, we reduce the spectral discrepancies between the RGB and the IR images with channel transformation as well as frequency-domain enhancement, so SEG images are generated. **Then**, we utilise a dual-stream weight-shareable network to extract features. **Finally**, identity loss and PABA loss are employed to supervise the whole learning process.

grained level, using specific pseudo-anchor of each modality to attract hetero-modality features of same instances and push away the features of different instances. The use of PABA enable the network to capture more fine-grained modality-consistent representations while emphasising discriminative identity embeddings. The main contributions of this paper are summarised as follows:

- We propose a simple yet efficient strategy for spectral enhancement. For the first time, frequency-domain and greyscale information are used simultaneously to reduce cross-modality discrepancies.
- We introduce a novel cross-modality constraint, PABA, which explores fine-grained coherence representations while retaining intrinsic discriminative information.
- Experimental results on the SYSU-MM01 [21] and RegDB [20] datasets demonstrate that our method outperforms other state-of-the-art methods.

II. METHOD

In this section, we first provide a detailed description of the spectral enhancement process. Then, we introduce the dual-stream structure for modality features extraction. Finally, we explain the working mechanism of the PABA loss. Fig. 2 demonstrates the overall architecture of our proposed method.

A. Semantically Enhanced Grey Images Generation

Infrared images contain more silhouette detail, while visible images contain more color information [14, 15, 31, 32, 33,

34, 35, 36, 37]. As shown in Fig. 3, we introduce an end-to-end spectral feature enhancement strategy aiming at efficiently generating images that approximate the infrared modality from visible images. This strategy reduces the large spectral gap while preserving complete pedestrian features. Concretely, given a visible image Y_{vis} containing R , G , and B channels, we introduce a transformation function $\tau(\cdot)$ to traverse each channel and generate the greyscale image Y_{grey} , and then replicate it to three channels (get Y_{grey3}) in order to match the input infrared images. The above process can be formulated as:

$$Y_{vis}(R, G, B) \xrightarrow{\tau(\cdot)} Y_{grey} \xrightarrow{copy} Y_{grey3}, \quad (1)$$

$$\tau(x) = \alpha \cdot R(x) + \beta \cdot G(x) + \gamma \cdot B(x), \quad (2)$$

where the values of (α, β, γ) tuple are $(0.299, 0.587, 0.114)$. In addition, several studies have demonstrated that the phase component of Fourier transform contains high-level semantic information, such as body silhouettes [16, 17, 18]. Inspired by this, we extract the phase information from the frequency domain to enhance the silhouette representation. The generation of semantically enhanced grey image Y_{seg} can be represented as:

$$X_{pha}, X_{amp} = \mathcal{F}_{FFT}(Y_{vis}), \quad (3)$$

$$Y_{seg} = \mathcal{F}_{IFFT}(X_{pha}) + Y_{grey3}, \quad (4)$$

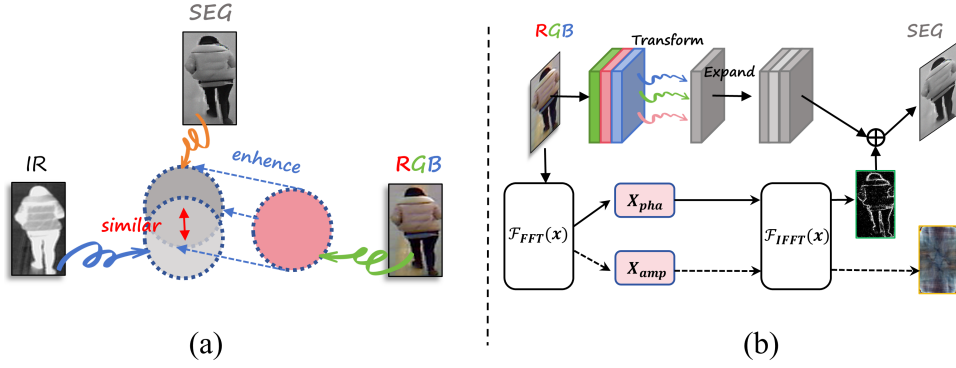


Fig. 3. (a) We perform spectral feature enhancement by converting visible/RGB image into SEG image, and the enhanced image is similar in style to infrared (IR) image. (b) Details of SEG image generation.

where $\mathcal{F}_{\text{FFT}}(\cdot)$ and $\mathcal{F}_{\text{IFFT}}(\cdot)$ denote the Fourier transform and its inverse operation, respectively, and X_{pha} and X_{amp} represent the phase and amplitude components.

B. Weight-Shareable Dual-Stream Network

To alleviate the remaining modality discrepancies between SEG and IR images, we employ a weight-shareable dual-stream network to extract shared modality representations while preserve the specific modality cues. Specifically, the infrared image input is denoted as $Y_{ir} \in \mathbb{R}^{H \times W \times C}$ (H , W , and C denote height, width, and channel, respectively), we apply the first three layers of ResNet-50 [19] with shared weights to extract the shared features of Y_{seg} and Y_{ir} . This process can be represented as the following arithmetic operations:

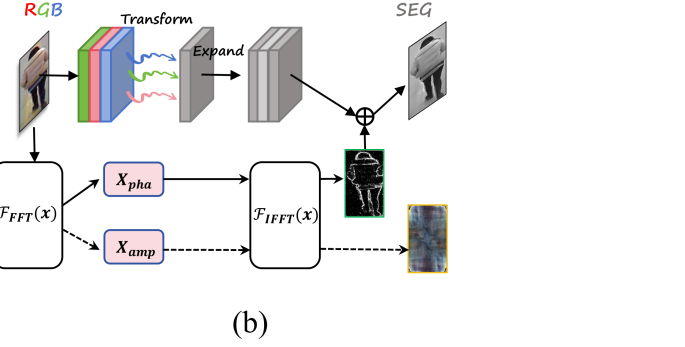
$$F_{\text{shared}} = \text{Conv}_{\text{res}}^3(\text{Conv}_{\text{res}}^2(\text{Conv}_{\text{res}}^1([Y_{ir}, Y_{seg}]_o^b))), \quad (5)$$

$$F_{\text{shared}}^{\text{seg}}, F_{\text{shared}}^{\text{ir}} = [F_{\text{shared}}]_h^b, \quad (6)$$

where $[\cdot]_o^b$ and $[\cdot]_h^b$ represent the **c**Oncatenation and **c**Hunking operations along the **b**atch dimension. In addition, we duplicate the last layer of ResNet-50 to extract higher-level modality-specific cues $F_{\text{specific}}^{\text{seg}}$ and $F_{\text{specific}}^{\text{ir}}$. Unlike previous methods [5, 6, 7, 8, 9, 10, 11, 12, 13, 38], the designed structure introduce only one additional layer for cross-modality feature extraction, which avoids extensive computational overhead.

C. Pseudo Anchor-Guided Bidirectional Aggregation Loss

To further mine modality-consistent representations while maintaining the discrimination of inter-class features, we propose a Pseudo Anchor-guided Bidirectional Aggregation (PABA) loss. It sets a pseudo-anchor for each modality to attract samples from the opposite modality. Compared to the standard triplet loss [30], the PABA loss can effectively reduce the intra-class cross-modality discrepancies. Specifically, we split $F_{\text{shared}}^{\text{seg}}$ and $F_{\text{shared}}^{\text{ir}}$ into N horizontal parts and obtain chunking features $F_{\text{shared}}^{\text{seg}} = [f_1^{\text{seg}}, f_2^{\text{seg}}, \dots, f_N^{\text{seg}}]$ and $F_{\text{shared}}^{\text{ir}} = [f_1^{\text{ir}}, f_2^{\text{ir}}, \dots, f_N^{\text{ir}}]$. The PABA loss can be formulated as follows:



$$L_{PABA}^{(Ma, Mb)}(i) = \frac{1}{K} \sum_{p=1}^K \max([\max D(pf_{i,p}^{Ma}, f_{i,p}^{Mb}) - \min_{p \neq q} D(pf_{i,p}^{Ma}, f_{i,q}^{Mb}) + \text{margin}], 0), \quad (7)$$

$$L_{PABA}^{\equiv} = \sum_{i=1}^N (L_{PABA}^{(\text{seg}, \text{ir})}(i) + L_{PABA}^{(\text{ir}, \text{seg})}(i)), \quad (8)$$

where Ma and Mb represent different modality categories and K is the number of identities. $pf_{i,p}$ denotes the pseudo-anchor from i -th part, which is the arithmetic centre of features with same identity and modality in a mini batch.

We achieve cross-modality bidirectional aggregation within each set of chunking features. Compared to the cross-centre loss in [9, 10, 11], this fine-grained design leads to a more compact modality-consistent representations. In addition, we adopt cross-entropy loss as the identity (ID) loss to supervise the modality-specific features as well as the chunking features, and the total loss can be denoted as:

$$L_{\text{ALL}} = \lambda_1 \cdot L_{\text{ID}}^{\text{specific}} + \lambda_2 \cdot L_{PABA}^{\equiv} + \lambda_3 \cdot \sum_{i=1}^N L_{\text{ID}}^{\text{chunks}}(i) \quad (9)$$

where λ_1 , λ_2 , and λ_3 are hyper-parameters to balance the weight of each loss function.

III. EXPERIMENTS

A. Datasets, Evaluation Protocols, and Implementation

Datasets. The performance of SEPG-Net is evaluated on two public benchmark VI-ReID datasets: RegDB [20] and SYSU-MM01 [21]. The RegDB dataset contains 402 identities, with each identity represented by 10 visible and 10 infrared images. RegDB has two test modes: V-2-I (visible-to-infrared) and I-2-V (infrared-to-visible). The SYSU-MM01 dataset is collected with 6 cameras (3 from indoor and 3 from outdoor), comprising a total of 302,420 visible and infrared images from 491 identities. The test modes of SYSU-MM01 are categorized as All-search and Indoor-search.

TABLE I
THE COMPARISON RESULTS OF SEPG-NET AND STATE-OF-THE-ART METHODS ON REGDB AND SYSU-MM01 DATASETS.

Method	Venue	RegDB				SYSU-MM01			
		V-2-I		I-2-V		All-search		Indoor-search	
		Rank-1	mAP	Rank-1	mAP	Rank-1	mAP	Rank-1	mAP
AlignGAN [5]	ICCV 19	57.9	53.6	56.3	53.4	42.4	40.7	45.9	54.3
X-Modal [6]	AAAI 20	62.2	60.2	-	-	49.9	50.7	-	-
NFS [23]	CVPR 21	80.5	72.1	77.9	69.8	56.9	55.5	62.7	69.8
FMCNet [24]	CVPR 22	89.1	84.4	88.4	83.9	66.3	62.5	68.2	74.1
CMIT [12]	TMM 23	88.8	88.5	84.6	83.6	70.9	65.5	73.3	77.2
SFANet [25]	TNNLS23	76.3	68.0	70.2	63.8	65.7	60.8	71.6	80.1
PMWGCN [26]	TIFS 24	90.6	84.5	88.8	81.6	66.8	64.9	72.6	76.2
CAJ [27]	TPAMI 24	85.7	79.7	84.9	77.8	71.5	68.2	78.4	82.0
DARD [28]	TIFS 24	86.2	85.4	85.5	85.1	69.3	65.7	79.6	60.3
DCPLNet [13]	TII 24	94.2	87.3	91.7	84.8	74.0	70.4	78.3	81.9
Ours*	-	97.7	90.8	95.8	90.4	76.4	71.3	84.5	86.2

*Red and blue represent the best and second-best results, respectively.

TABLE II
ABLATION EXPERIMENTS OF SEPG-NET ON SYSU-MM01 DATASET (ALL-SEARCH MODE).

baseline	+SE	+CC	+PABA	Rank-1	mAP
✓				69.6	66.8
✓	✓			72.3	69.4
✓	✓	✓		73.8	69.7
✓	✓		✓	76.4	71.3

Evaluation Protocols. Following the standard practices in the ReID community [1, 2, 3, 4, 5], we utilize Rank-1 (Probability that the query target appears first in the query results) and mAP (mean Average Precision) to comprehensively evaluate the performance of SEPG-Net and other baseline methods.

Implementation Details. Our SEPG-Net employs a ResNet-50 [18] as the backbone, pre-trained on ImageNet [22]. The network is deployed on the Nvidia RTX 4090 GPU for training and testing. In the training phase, each minibatch contains 8 identities, and each identity represented by 7 visible and 7 infrared images. We set the initial learning rate to 0.03, and it decays at the 30th and 70th epoch by a factor of 0.1 (120 epochs in total). The number of horizontal chunks N is set to 12. The values of the parameters $margin$, λ_1 , λ_2 , and λ_3 are set to 0.5, 1, 2.5, and 1, respectively.

B. Comparison With State-of-the-Art Methods

To validate the effectiveness of SEPG-Net, several state-of-the-art methods are introduced for comparison [5, 6, 12, 13, 23, 24, 25, 26, 27, 28]. Table I reports the optimal performance achieved by the proposed SEPG-Net, which surpasses the second-best method on the RegDB dataset by 3.5% and 4.1% in Rank-1 and by 2.3% and 5.3% for mAP in V-2-I and I-2-V modes, respectively. Moreover, SEPG-Net achieves the best results on the SYSU-MM01 dataset. This performance can be attributed to two key factors: i) The transformation from RGB to SEG effectively reduce the modality discrepancies at the data level; ii) More fine-grained consistent embeddings are explored by guiding local cross-modality alignment through pseudo anchors. These experimental results strongly demonstrate the superiority of SEPG-Net.

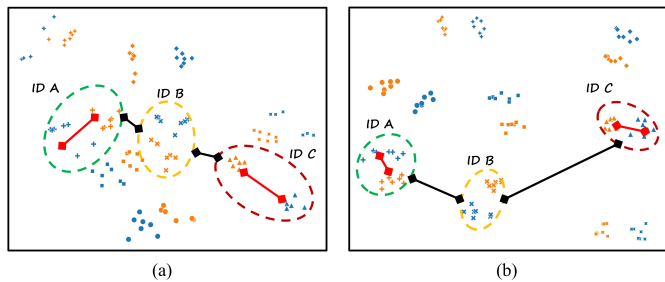


Fig. 4. t-SNE feature visualisation of baseline (a) and SEPG-Net (b) on SYSU-MM01. Blue and orange represent the infrared and visible modalities, respectively.

C. Ablation Study

We also conduct ablation experiments, as shown in Table II. The experimental setups are as follows: the baseline includes only the dual-stream backbone supervised with the ID loss. The terms of +SE, +CC and +PAPB represent the application of spectral enhancement, cross-centre loss [9] and PABA loss, respectively. As observed, the baseline achieves 69.6% Rank-1 and 66.8% mAP on the SYSU-MM01 dataset (All-search mode). When the proposed spectral enhancement strategy is utilized to reduce the cross-modality gap, the performance improves by 2.7% Rank-1 and 2.6% mAP. Moreover, we compare the classical cross-centre loss with the proposed PABA loss, showing that the PABA leads to an additional 2.6% improvement in Rank-1 and a 1.6% gain in mAP compared to the cross-centre loss. Furthermore, the t-SNE [29] feature visualisation results in Fig. 4 demonstrate that SEPG-Net encourages more compact modality-consistent representations while increasing inter-class discrimination.

IV. CONCLUSION

SEPG-Net, a simple yet effective architecture, is developed for VI-ReID task. First, we observe and analyse the spectral discrepancies between infrared and visible images and propose an end-to-end spectral enhancement strategy which uses frequency domain information and greyscale space to bridge the gap from RGB images to infrared images. Furthermore, we rethink the cross-modality learning process of previous VI-ReID approaches and propose a PABA loss paradigm, which endeavours to promote cross-modality bidirectional aggregation at a fine-grained level while preserving discriminative identity information. We compare SEPG-Net's performance with other well-known methods on the RegDB and SYSU-MM01 datasets, and conduct ablation experiments on our key designs. The experimental results demonstrate that SEPG-Net outperforms state-of-the-art methods.

V. ACKNOWLEDGEMENT

This work was supported by National Nature Science Foundation of China (grant no. U21A6003). ([†]Zhihao Chen and Yiyuan Ge contribute equally to this work) (*Corresponding author: Ziyang Wang.)

REFERENCES

- [1] He S, Luo H, Wang P, et al. Transreid: Transformer-based object re-identification[C] CVPR. 2021: 15013-15022.
- [2] Z. Chen and Y. Ge, "Part-Attention Based Model Make Occluded Person Re-Identification Stronger," 2024 International Joint Conference on Neural Networks (IJCNN), Yokohama, Japan, 2024, pp. 1-8, doi: 10.1109/IJCNN60899.2024.10650499.
- [3] Ge Y, Yu M, Chen Z, et al. Semantically enhanced attention map-driven occluded person re-identification[J]. Electronics Letters, 2024, 60(9): e13217.
- [4] Chen Z, Ge Y, Yue Q. Features Reconstruction Disentanglement Cloth-Changing Person Re-identification[C]//International Conference on Intelligent Computing. Singapore: Springer Nature Singapore, 2024: 390-403.
- [5] Wang G, Zhang T, Cheng J, et al. RGB-infrared cross-modality person re-identification via joint pixel and feature alignment[C] ICCV. 2019: 3623-3632.
- [6] Li D, Wei X, Hong X, et al. Infrared-visible cross-modal person re-identification with an x modality[C] AAAI. 2020, 34(04): 4610-4617.
- [7] Choi S, Lee S, Kim Y, et al. Hi-CMD: Hierarchical cross-modality disentanglement for visible-infrared person re-identification[C] CVPR. 2020: 10257-10266.
- [8] Qian Y, Tang S K. Pose Attention-Guided Paired-Images Generation for Visible-Infrared Person Re-Identification[J]. IEEE SPL, 2024.
- [9] Zhu Y, Yang Z, Wang L, et al. Hetero-center loss for cross-modality person re-identification[J]. Neurocomputing, 2020, 386: 97-109.
- [10] Liu H, Tan X, Zhou X. Parameter sharing exploration and hetero-center triplet loss for visible-thermal person re-identification[J]. IEEE TMM, 2020, 23: 4414-4425.
- [11] Hao X, Zhao S, Ye M, et al. Cross-modality person re-identification via modality confusion and center aggregation[C] ICCV. 2021: 16403-16412.
- [12] Feng Y, Yu J, Chen F, et al. Visible-infrared person re-identification via cross-modality interaction transformer[J]. IEEE TMM, 2022, 25: 7647-7659.
- [13] Chan S, Meng W, Bai C, et al. Diverse-Feature Collaborative Progressive Learning for Visible-Infrared Person Re-Identification[J]. IEEE TII, 2024.
- [14] Feng Z, Lai J, Xie X. Learning modality-specific representations for visible-infrared person re-identification[J]. IEEE TIP, 2019, 29: 579-590.
- [15] Zhang L, Du G, Liu F, et al. Global-local multiple granularity learning for cross-modality visible-infrared person reidentification[J]. IEEE TNNLS, 2021.
- [16] Oppenheim A V, Lim J S. The importance of phase in signals[J]. IEEE, 1981, 69(5): 529-541.
- [17] Piotrowski L N, Campbell F W. A demonstration of the visual importance and flexibility of spatial-frequency amplitude and phase[J]. Perception, 1982, 11(3): 337-346.
- [18] Xu Q, Zhang R, Zhang Y, et al. A fourier-based framework for domain generalization[C] CVPR. 2021.
- [19] He K, Zhang X, Ren S, et al. Deep residual learning for image recognition[C] CVPR. 2016: 770-778.
- [20] Wu A, Zheng W S, Yu H X, et al. RGB-infrared cross-modality person re-identification[C] ICCV. 2017: 5380-5389.
- [21] Nguyen D T, Hong H G, Kim K W, et al. Person recognition system based on a combination of body images from visible light and thermal cameras[J]. Sensors, 2017, 17(3): 605.
- [22] Deng J, Dong W, Socher R, et al. Imagenet: A large-scale hierarchical image database[C] CVPR, 2009: 248-255.
- [23] Chen Y, Wan L, Li Z, et al. Neural feature search for rgb-infrared person re-identification[C] CVPR. 2021.
- [24] Zhang Q, Lai C, Liu J, et al. Fmcnet: Feature-level modality compensation for visible-infrared person re-identification[C] CVPR. 2022: 7349-7358.
- [25] Liu H, Ma S, Xia D, et al. SFANet: A spectrum-aware feature augmentation network for visible-infrared person reidentification[J]. TNNLS, 2021, 34(4): 1958-1971.
- [26] Sun R, et al. Robust Visible-Infrared Person Re-Identification based on Polymorphic Mask and Wavelet Graph Convolutional Network[J]. IEEE TIFS, 2024.
- [27] M. Ye, Z. Wu, C. Chen and B. Du, "Channel Augmentation for Visible-Infrared Re-Identification," in IEEE TPAMI, vol. 46, no. 4, pp. 2299-2315, April 2024.
- [28] Z. Wei, X. Yang, N, et al. "Dual-Adversarial Representation Disentanglement for Visible Infrared Person Re-Identification," in IEEE TIFS, vol. 19, pp. 2186-2200, 2024.
- [29] Van der Maaten L, Hinton G. Visualizing data using t-SNE[J]. Journal of machine learning research, 2008, 9(11).
- [30] Schroff F, Kalenichenko D, Philbin J. Facenet: A unified embedding for face recognition and clustering[C] CVPR. 2015: 815-823.
- [31] Zhuang J, Zheng Y, Guo B, et al. Globally Deformable Information Selection Transformer for Underwater Image Enhancement[J]. IEEE Transactions on Circuits and Systems for Video Technology, 2024.
- [32] Zhuang J, Chen W, Guo B, et al. Infrared Weak Target Detection in Dual Images and Dual Areas[J]. Remote Sensing, 2024, 16(19): 3608.
- [33] Feng T, Wang X, Han F, et al. U2udata: A large-scale cooperative perception dataset for swarm uavs autonomous flight[C]//Proceedings of the 32nd ACM International Conference on Multimedia. 2024: 7600-7608.
- [34] Zou S, Zhang Z, Gao G. OCTAMamba: A State-Space Model Approach for Precision OCTA Vasculature Segmentation[J]. arXiv preprint arXiv:2409.08000, 2024.
- [35] Xiao X, Wang W, Xie J, et al. HGTDP-DTA: Hybrid Graph-Transformer with Dynamic Prompt for Drug-Target Binding Affinity Prediction[J]. arXiv preprint arXiv:2406.17697, 2024.
- [36] Wang W, Xiao X, Liu M, et al. Multi-dimension Transformer with Attention-based Filtering for Medical Image Segmentation[J]. arXiv preprint arXiv:2405.12328, 2024.
- [37] Shi, Jun, et al. "Sandformer: CNN and Transformer under Gated Fusion for Sand Dust Image Restoration." ICASSP 2023-2023 IEEE International Conference on Acoustics, Speech and Signal Processing (ICASSP). IEEE, 2023.
- [38] Lyu S, Zhou X, Hu X. Multi-view Hypergraph-based Contrastive Learning Model for Cold-Start Micro-video Recommendation[J]. arXiv preprint arXiv:2409.09638, 2024.